Macroalgal influence on particulate organic matter sources and early transformation in an Arctic fjord

Ashok S Jagtap[1], Archana Singh[1], Anand Jain[1], Nandini Raj[2], Manish Tiwari[1]

[1]National Centre for Polar and Ocean Research, Ministry of Earth Sciences, Vasco-da-Gama, Goa 403804, India

[2]Amity Institute of Biotechnology, Amity University, Uttar Pradesh 201313, India

Correspondence to:

Ashok S. Jagtap (ashokjagtap200@gmail.com),

Archana Singh (archanasingh@ncpor.res.in)

Highlights

- Macroalgal-dominated sites were observed with higher labile surface particulate organic carbon and nitrogen signatures compared to adjacent waters.
- Biochemical and biomolecular composition indicated lateral transport from macroalgal-beds with conservative reorganization.
- Brandal was identified as a model site for future biogeochemical studies related to macroalgal expansion in Kongsfjorden.

Abstract

Accelerated Arctic warming is promoting the expansion of coastal macroalgal habitats; yet their influence on pelagic organic carbon cycling remains unresolved. This study investigates the influence of macroalgal beds on the biochemical composition of surface particulate organic matter (POM) in Kongsfjorden, Svalbard, during late summer 2023. Surface waters were sampled at four macroalgal-dominated sites (MDS) and from adjacent waters (Adj-W) located 500 m and 1500 m away. A multi-proxy approach integrating elemental composition, stable isotopes, biopolymeric fractions, monosaccharides, and amino acids was used to trace macroalgal contributions and their lateral redistribution. Concentrations of particulate organic carbon, nitrogen, carbohydrates, and proteins were consistently higher at MDS than in Adj-W, indicating localized enrichment of biochemically labile organic matter within macroalgal habitats. Molecular analyses further revealed elevated concentrations of macroalgal-associated sugars (glucose, galactose, fucose, mannuronic acid) and labile amino acids (Asp, Glu, Gly, Ser, Ala) reinforcing macroalgal-derived contributions to surface POM. While $\delta^{13}C_{POC}$ showed minimal spatial variation (−26.8 to −29.1‰), the biochemical and molecular signatures indicated a decreasing macroalgal contribution towards Adj-W, along with internal reorganization, suggesting lateral transport of macroalgal-derived POM with selective early-stage transformation. Overall, these findings indicate that Arctic macroalgal beds act as dynamic coastal biogeochemical hotspots, redistributing and transforming organic carbon beyond their habitat.

Keywords: Arctic fjords; macroalgal-derived organic matter; coastal carbon cycling; lateral transport

1. Introduction

Accelerated warming of the Arctic has led to pronounced environmental changes, including a reduction in sea ice extent and thickness, intensified glacier melt, widespread permafrost thawing, and a shift toward more liquid precipitation (Dai et al., 2019; Rantanen et al., 2022). These changes are altering marine primary production (Attard et al., 2024), coastal carbon sources (Mathew et al., 2025), and nutrient dynamics within Arctic fjord systems (McGovern et al., 2020). Amid these environmental transformations, macroalgae have demonstrated ecological resilience and adaptability, enabling their expansion along Arctic coastlines (Assis et al., 2022). Recent estimates from species distribution modeling indicate a substantial increase in subtidal (45%) and intertidal (8%) brown macroalgal cover along the Arctic coastline over the past few decades (Krause-Jensen et al., 2020). This rapid and ongoing macroalgal expansion contributes substantially to coastal primary productivity and carbon dynamics in the Arctic (Attard et al., 2024; Krause-Jensen et al., 2020). Macroalgal biomass and condition are strongly shaped by local environmental variability, with runoff and site-specific forcing influencing kelp biochemistry and ecosystem functioning in Arctic coastal systems (Castro de la Guardia et al., 2025; Niedzwiedz et al., 2025). Comparable environment-driven changes in kelp biomass and distribution have been reported across the Arctic, including Greenland and the Canadian Arctic, indicating pan-Arctic rather than site-specific responses (Carlson et al., 2026; Filbee-Dexter and Wernberg, 2020; Krause-Jensen and Duarte, 2016). Kelp forest structure shifted markedly, with a reduced depth distribution, a declining abundance of several kelp species, and an increasing dominance of *Alaria esculenta*, driven primarily by rising turbidity and coastal darkening rather than temperature alone, thereby reshaping kelp biomass, demography, and ecosystem functioning in Kongsfjorden (Düsedau et al., 2024). Field experiments have also shown that macroalgal blades can lose approximately 3% of

their total area per day due to mechanical stress, physical abrasion against rocky substrates, seasonal increases in tissue brittleness, and biological weakening by epiphytes. These processes provide a substantial and continuous input of macroalgal-derived material to the coastal particulate organic matter (POM) pool (Buchholz and Wiencke, 2016).

Macroalgal beds contribute a significant amount of macroalgal-derived organic carbon, approximately 60% as particulate organic carbon (POC), and approximately 30% as dissolved organic carbon (DOC) (Kennedy and Blain, 2025; Pessarrodona et al., 2022) to the surrounding environment, and play a crucial role in supporting secondary production via detrital food web and coastal Arctic carbon cycling (Pedersen et al., 2021; Renaud et al., 2015; Simpkins et al., 2025). Macroalgal POM appears in multiple forms, including whole thalli and tissue fragments, and is often buoyant due to structural features such as pneumatocysts, allowing particles to stay suspended in surface waters (Carlson et al., 2026; Kennedy and Blain, 2025). This buoyancy promotes extensive lateral transport across coastal and fjord systems, effectively linking benthic macroalgal production with pelagic environments and shaping the spatial distribution of organic carbon (Carlson et al., 2026; van der Mheen et al., 2024). A substantial fraction of the carbon produced in macroalgal beds is exported to surrounding environments, with only about 2% remaining and settling at the site of production (Kennedy and Blain, 2025; Krause-Jensen and Duarte, 2016; Pessarrodona et al., 2022). Macroalgal POM undergoes microbial-mediated transformation and degradation during transit and thereby affects biogeochemical processes in macroalgal beds as well as adjacent waters (Adj-W) (Duarte et al., 2013; Krause-Jensen and Duarte, 2016; Ortega et al., 2019). Biochemical compositional and lipid biomarker studies have shown hints of macroalgal contribution to POM (Singh et al., 2024b) and sediments (Roy et al., 2025) in Kongsfjorden. Similarly, studies from saline lake systems demonstrate that microbial

transformations of organic matter require high-resolution molecular proxies to distinguish carbon sources (Jiang et al., 2022; Yang et al., 2020). However, the spatial variability and magnitude of macroalgal-derived organic carbon contributions to POM along coastal gradients remain poorly understood.

To better resolve the sources and transformation pathways, and to understand how the expansion of macroalgal forests will influence Arctic coastal biogeochemistry, a systematic biochemical characterization of POM in and around macroalgal-dominated sites is necessary. Thus, the present study investigated the biochemical composition of POM from the surface waters of Kongsfjorden (Svalbard) at four macroalgal-dominated sites (MDS), and their respective adjacent waters (Adj-W) located 500 m and 1500 m from the MDS sites. Here, we addressed three key questions: (i) To what extent do the biochemical characteristics of surface POM at MDS reflect inputs from macroalgal-derived organic matter? (ii) How does the biochemical composition of POM changes from MDS to Adj-W, and (iii) What do these changes reveal about the lateral transport and early alteration of macroalgal-derived organic matter?

Material and Methods

2.1 Sampling site and locations

Surface water samples were collected during late summer 2023 (September–October) from four MDS distributed along and across the Kongsfjorden coast using the workboat Teisten, with a Niskin sampler deployed at 3 m depth, as well as from adjacent locations (Adj-W) located 500 m and 1500 m away from each MDS site (Figs. 1A and 1B). The seawater was pre-filtered using a 200 µm mesh to remove larger particles. Seawater samples (3 L) were filtered using pre-combusted (4 hours at 450 °C) 0.7 µm pore size glass fiber filters (GF/F) to collect particulate matter.

Immediately after filtration, the GF/F filters were stored at -80 °C until analysis. An aliquot of 100 mL seawater sample for dissolved nutrients analysis was collected in high-density polyethylene bottles from each sampling location and stored at -80 °C until analysis.

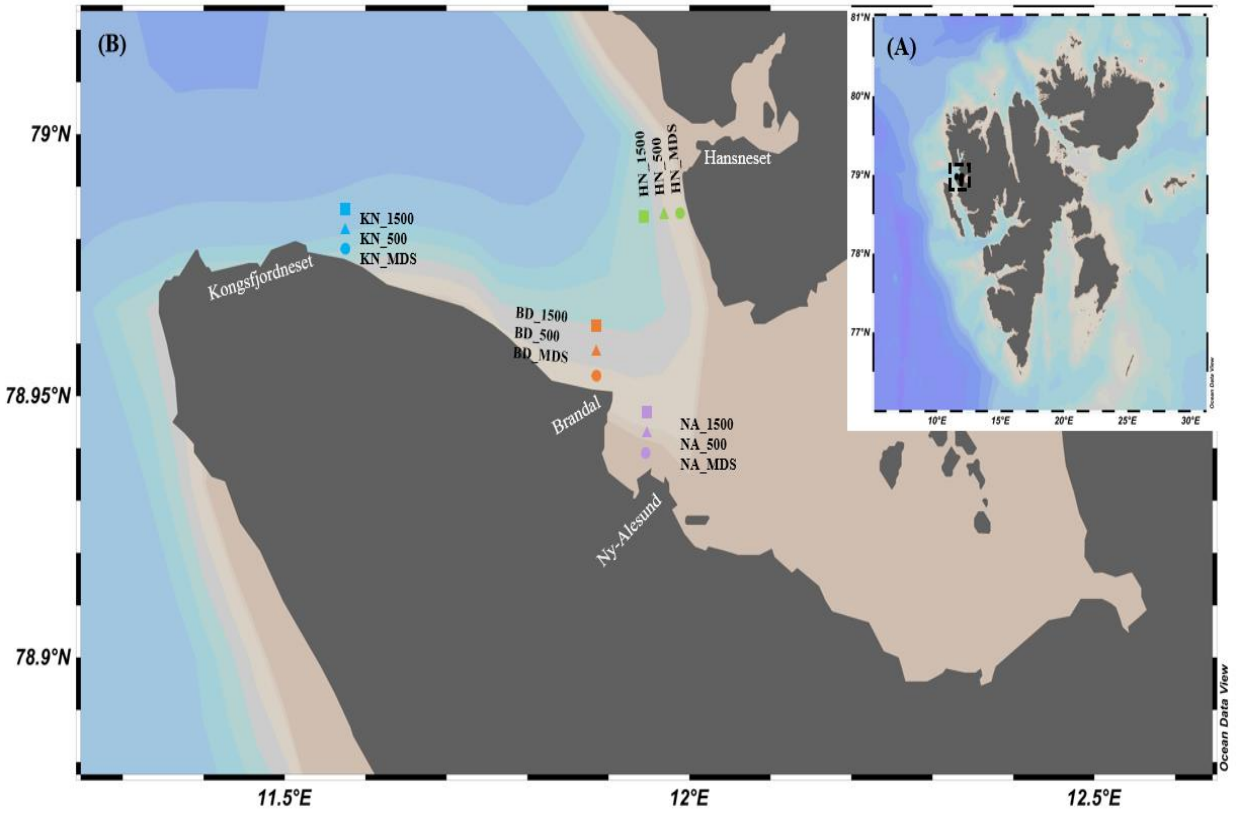

Figure 1. Study area and sampling locations in Svalbard (A) and the detailed map of sampling stations in Kongsfjorden (B) across nearshore macroalgal beds (MDS), mid-fjord (500 m), and offshore (1500 m) sites at BD, NA, KN, and HN.

2.2 Physicochemical characteristics of seawater

The vertical profiles of temperature, salinity, and turbidity at each sampling location were recorded using an SBE 911 plus instrument (Seabird Electronics Inc., USA). The concentrations of dissolved nutrients (nitrate, nitrite, silicate, and phosphate) were determined using a Seal AA3 analytical auto-analyzer with a standard deviation of ±1% and an R^2 value of >0.99 (Grasshoff et

al., 2009). Chlorophyll *a* was extracted following (Singh et al., 2024a) with minor modifications. Briefly, GF/F filters were extracted in 90% acetone under low-light conditions by keeping them overnight at −20 °C. The pigment extracts were centrifuged (10,000×g, 4 °C, 10 min), filtered (0.2 µm PVDF), and analyzed using an Agilent 1200 HPLC with a ZORBAX 300 Extend-C8 column (1.1 mL min^{-1}, 40 °C). Pigments were separated using a reverse-phase methanol–ammonium acetate gradient and identified by comparing retention times and absorption spectra (250–850 nm) against a DHI chlorophyll-a standard.

2.3 Elemental and isotopic analyses of POM

Filters containing particulate matter were dried at 45 °C for 24 h, after which carbonates were removed by exposing the filters to fumes of 35% HCl for 6 h in a desiccator. The treated filters were then weighed and tightly packed into tin capsules for elemental and isotopic analyses (Jain et al., 2019; Singh et al., 2024b). Particulate nitrogen (PN), particulate organic carbon (POC), δ^{13}C-POC, and δ^{15}N-PN were measured at the Marine Stable Isotope Laboratory, National Centre for Polar and Ocean Research, Goa, India, using an elemental analyzer coupled to an isotope ratio mass spectrometer (EA-IRMS; Isoprime Vario Isotope Cube) operated in continuous-flow mode. External analytical precision for δ^{13}C and δ^{15}N was ±0.10‰ and ±0.14‰ (1σ), respectively, determined by repeated analysis of caffeine (IAEA-600) and ammonium sulphate (IAEA-N1) standards. δ^{13}C and δ^{15}N values are reported relative to VPDB and Air-N_2, respectively, with ammonium sulfate (IAEA-N1) used for normalization to Air-N_2. External precision for %C and %N was ±0.96% and ±0.95% (1σ), respectively, based on repeated measurements of sulfanilamide.

2.4 Biochemical analysis of POM

The dried, pre-weighed filters with POM were cut into smaller pieces using clean stainless-steel scissors and then used for further analysis. The total particulate carbohydrates (P-CHO), particulate proteins (P-PRT), and particulate lipids (P-LIP) were analyzed using the phenol-sulfuric acid (Dubois et al., 1956), Lowry (Upreti et al., 1988), and Phosphovanillin (Folch et al., 1957) methods, respectively, and as described earlier in (Singh et al., 2024b). Biopolymeric carbon (BPC) was determined as depicted by (Danovaro et al., 2001), using the sum of the carbon equivalents of P-CHO, P-PRT, and P-LIP (conversion factors of 0.4, 0.49 and 0.75, respectively).

2.5 Monosaccharide composition analysis of POM

For monosaccharide analysis, POM samples were acid-hydrolyzed and then analyzed using High-Performance Anion Exchange Chromatography coupled with a Pulsed Amperometric Detector (HPAEC-PAD) as described earlier by (Singh et al., 2024a). In brief, GF/F filters with POM were treated with 1 mL of 12 M H_2SO_4 at 25 °C for 2 h, diluted to 1.2 M with Milli-Q water, purged with N_2, sealed, and incubated at 100 °C for 4 h. After cooling, the internal standard (myo-inositol) was added, and the samples were neutralized with pre-combusted $CaCO_3$, centrifuged (6000 rpm, 10 min), and filtered (0.22 µm PTFE). The samples were analyzed using HPAEC-PAD (Metrohm 940 Professional IC Vario) equipped with an Au working electrode and Ag/AgCl reference electrode, on a Metrosep Carb 2 (250/4.0) coupled with a guard column at 30 °C. Sugars were separated using gradient elution (0.6 mL min^{-1}) with solvent A (1 mM NaOH, 1 mM sodium acetate) and solvent B (150 mM NaOH, 100 mM sodium acetate) over 120 min. Neutral sugars, amino sugars, and mannitol were resolved isocratically with solvent A, while acidic sugars were

separated using a solvent B gradient. Identification and quantification of monosaccharides were achieved using calibration with a mixture of sugar standards (Sigma-Aldrich, USA).

2.6 Amino acid composition analysis of POM

For amino acid analysis, POM samples were acid-hydrolyzed using HCl and then analyzed using High-Performance Liquid Chromatography coupled with a Diode Array Detector (HPLC-DAD) using the method outlined by (Kim et al., 2024). GF/F filters with POM were cut into small pieces, placed in Pyrex tubes with 10 mL of 6 M HCl, purged with N_2, sealed, and hydrolyzed at 110 °C for 22 h. After cooling, nor-leucine was added as an internal standard. The hydrolysate was centrifuged, freeze-dried, reconstituted in 1 mL of Milli-Q water, vortexed, and filtered (0.22 µm). Amino acids were derivatized by sequentially mixing 2.5 µL borate buffer with 1 µL sample (0.5 min), followed by addition of 1 µL OPA reagent, mixing, and dilution with 15.5 µL of Milli-Q water in the HPLC (Agilent 1200) autosampler prior to injection. HPLC separation of the derivatized amino acids was carried out using a Zorbax AAA column (5 µm, 4.6 × 150 mm), a 20 µL injection volume, and a flow rate of 2 mL min^{-1}. Detection was performed using a DAD (Agilent) at 338 nm (reference 390 nm). The separation was carried out using gradient elution with mobile phase A (40 mM phosphate buffer, pH 8.2) and mobile phase B (acetonitrile: methanol:water, 45:45:10). Identification and quantification were performed using external calibration with a 17 amino acid standard mixture (Fig. S1: 10, 100, 250, 1000 pmol, Agilent, USA).

2.7 Statistical analysis

Statistical analysis were performed using R (version 4.6.0). Prior to analysis of variance (ANOVA) the assumptions of normality and homogeneity of variance were assessed using the Shapiro-Wilk and Levene's tests (Table S1). Pearson correlation analysis was performed at a significance level of 0.05 to examine the relationship between the variables. Principal component analysis (PCA) was employed using the vegan and factoextra packages to visualize the biogeochemical gradient, and all plots were generated using ggplot2.

3. Results

3.1 Salinity, temperature, nutrients, and chl-a

Surface seawater salinity exhibited spatial variation, with the lowest salinity (27.4±0.0 PSU) recorded at NA_1500 station, a site most influenced by glacier meltwater, and the highest salinity (31.6±0.1 PSU) observed at KN_MDS, the outermost site under the influence of oceanic circulation (Table 1). Surface seawater temperature was lowest (4.2±0.0 °C) at NA_500 and highest at KN_MDS (5.5±0.0 °C). The lowest turbidity (2.1±0.1 NTU) was recorded at both BD_MDS and HN_MDS, while maximum turbidity (7.4±0.0 NTU) was observed at KN_MDS.

Nitrate varied from 0.05 µM (BD_MDS) to 0.80 µM (NA_1500) and showed an increasing trend from MDS to Adj-W for NA, BD, and HN (Table 1). The overall average nitrate concentration was lower in MDS (0.39±0.23 µM) than in Adj-W (0.56±0.13 µM). Comparing different stations, the average nitrate concentration of all NA stations were high (0.66±0.12 µM), followed by KN (0.53±0.10 µM), HN (0.51±0.08 µM), and lowest at BD stations (0.30±0.22 µM). Nitrite concentration showed a similar pattern, with an increasing trend from MDS to Adj-W sites. However, phosphate concentrations showed minor differences (0.01 to 0.02 µM) among MDS and Adj-W sites.

Chlorophyll *a* (Chl *a*) concentrations ranged from 0.04 µg L^{-1} to 0.18 µg L^{-1} across all stations (Table 1) with no clear trend observed in other photosynthetic pigments (Table S2). Similar to nitrate, Chl *a* showed an increasing trend from MDS to Adj-W sites at the NA, BD, and HN stations, while KN exhibited relatively low concentrations at both MDS and Adj-W sites. Overall, the average Chl *a* concentration was lower at MDS (0.07 µg L^{-1}) compared to Adj-W (0.08 µg L^{-1}). Among stations, BD stations recorded the highest average Chl *a* concentrations (0.11 µg L^{-1}), followed by HN and NA with 0.07 µg L^{-1}, whereas KN (0.04 µg L^{-1}) stations exhibited the lowest average concentrations.

Table 1. Sampling stations and measured physicochemical parameters (temperature, salinity, nutrients, and chlorophyll a) across sampling stations.

Station	**Station depth** [m]	**Temperature** [ºC]	**Salinity** [PSU]	**Turbidity** [NTU]	**Nitrate** (µM)	**Phosphate** (µM)	**Nitrite** (µM)	**Chlorophyll a** [µg L^{-1}]
NA_MDS	3.5	5.0±0.1	31.3±0.0	3.5±0.4	0.58	0.18	0.09	0.09
NA_500	122	4.2±0.0	30.1±1.3	5.0±0.1	0.61	0.17	0.11	0.04
NA_1500	300	5.2±0.1	27.4±0.0	2.9±0.4	0.80	0.20	0.11	0.08
BD_MDS	6.7	5.1±0.0	29.9±0.0	2.1±0.1	0.05	0.13	0.01	0.09
BD_500	146	4.7±0.3	30.3±0.1	2.9±0.1	0.39	0.15	0.04	0.18
BD_1500	362	5.4±0.0	30.9±0.6	4.4±0.3	0.45	0.15	0.06	0.05
KN_MDS	3.4	5.5±0.0	31.6±0.1	7.4±0.0	0.49	0.14	0.06	0.05
KN_500	216	5.0±0.5	29.5±0.1	3.1±0.4	0.65	0.16	0.08	0.06
KN_1500	240	4.5±0.0	29.8±0.0	2.9±0.1	0.45	0.14	0.07	0.05
HN_MDS	4.5	4.5±0.2	28.7±1.8	2.1±0.1	0.43	0.14	0.04	0.06
HN_500	76	4.3±0.0	29.8±0.0	3.8±1.7	0.58	0.13	0.05	0.06
HN_1500	315	4.3±0.0	29.8±0.3	3.8±0.5	0.52	0.13	0.07	0.09

3.2 Elemental and stable isotopic composition

POC and PN concentrations varied over a wide range from 0.17 mg L^{-1} (KN_500) to 0.45 mg L^{-1} (BD_MDS) and from 0.04 mg L^{-1} (KN_500 and KN_1500) to 0.14 mg L^{-1} (BD_MDS), respectively (Fig. 2A). BD_MDS recorded the highest POC concentration (0.45 mg L^{-1}), followed by NA_MDS and HN_MDS (0.32 mg L^{-1}), with the lowest POC at KN_MDS (0.21 mg L^{-1}). Overall average POC and PN concentrations were higher at MDS (0.32±0.10 and 0.08±0.04 mg L^{-1}, respectively) than at Adj-W (0.26±0.08 and 0.06±0.02 mg L^{-1}), respectively. Across stations, mean POC was highest at BD (0.37±0.10 mg L^{-1}), followed by HN (0.32±0.01 mg L^{-1}) and NA (0.24±0.07 mg L^{-1}), and lowest at KN (0.19±0.02 mg L^{-1}) (Fig. 2B). A similar pattern was observed for PN, with the highest values at BD (0.10 ± 0.03 mg L^{-1}), followed by HN (0.07±0.01 mg L^{-1}), NA (0.06±0.00 mg L^{-1}), and KN (0.04±0.01 mg L^{-1}). The POC/PN ratio ranged from 2.9 (NA_1500) to 5.4 (NA_MDS). The POC/PN ratio showed an increasing trend from MDS to Adj-W for all stations, except NA (Fig. 2C). The NA station showed a decreasing trend in POC/PN ratio from MDS (5.4) to Adj-W (2.9) with the highest change of 2.5.

The $\delta^{13}C$ and $\delta^{15}N$ values of POM varied from −26.8‰ (NA_500) to −29.1‰ (KN_1500) and from 2.5 (KN_1500) to 15.9 (BD_1500), respectively. Mean $\delta^{13}C$ values of all MDS stations (−28.0±0.64‰) were similar to those of Adj-W stations (−28.1±0.67‰). However, individually KN showed a prominent decreasing trend in $\delta^{13}C$ (-27.1‰ to -29.1‰) and NA showed an increase of -28.5‰ to -27.5‰ from MDS to Adj-W, while HN and BD values were confined to a narrow range (-28.0‰ to -28.5‰). For $\delta^{15}N$, the overall average at MDS sites was lower (4.5 ± 0.73‰) than at Adj-W (6.4 ± 5.02‰). $\delta^{15}N$ value variations were minor (2.5‰ to 5.6‰) for the KN, HN, and NA stations, while the observed values for BD_500 (12.5‰) and BD_1500 (15.9‰) were quite high (Fig. 2B).

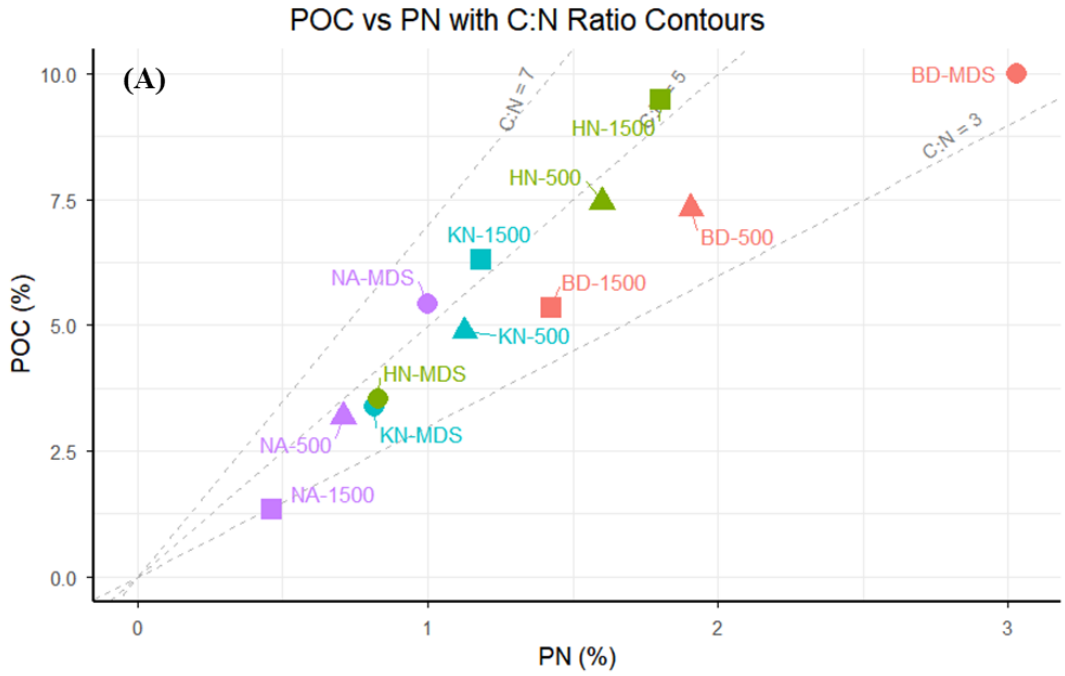
POC vs PN with C:N Ratio Contours
(A)
C:N = 7
C:N = 5
C:N = 3
BD-MDS
HN-1500
HN-500
BD-500
KN-1500
NA-MDS
BD-1500
KN-500
HN-MDS
KN-MDS
NA-500
NA-1500
POC (%)
PN (%)
10.0
7.5
5.0
2.5
0.0
0
1
2
3

256

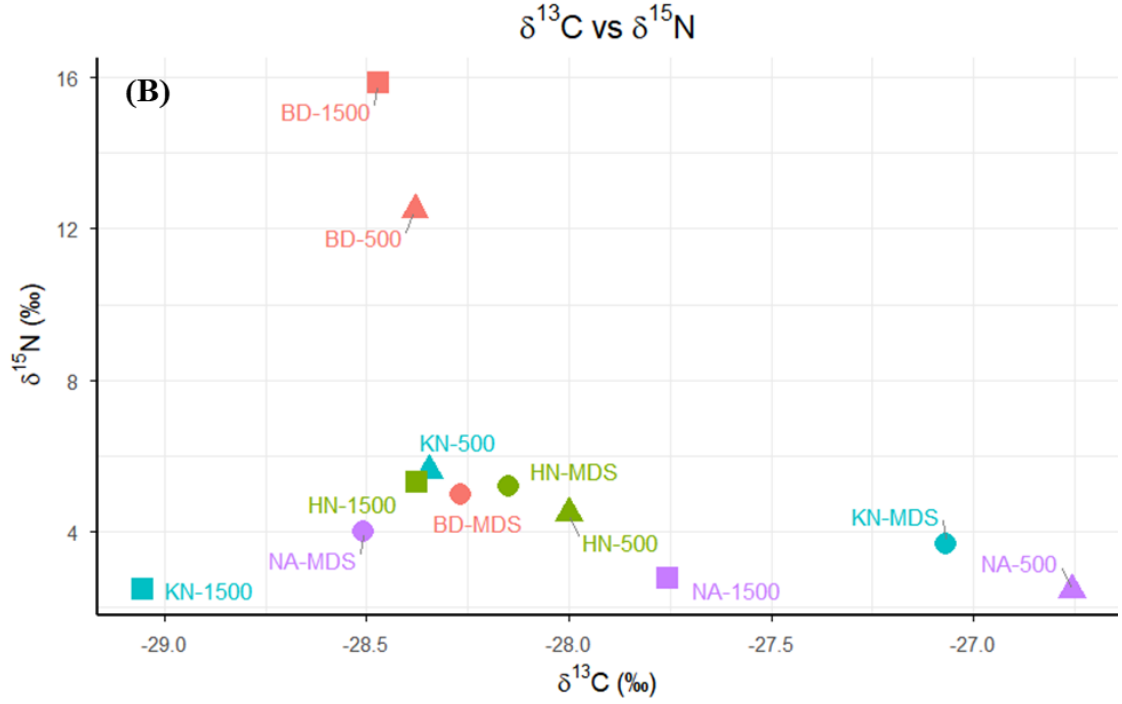
δ13C vs δ15N
(B)
BD-1500
BD-500
KN-500
HN-MDS
HN-1500
BD-MDS
HN-500
KN-MDS
NA-MDS
NA-500
KN-1500
NA-1500
δ15N (‰)
δ13C (‰)
16
12
8
4
-29.0
-28.5
-28.0
-27.5
-27.0

257

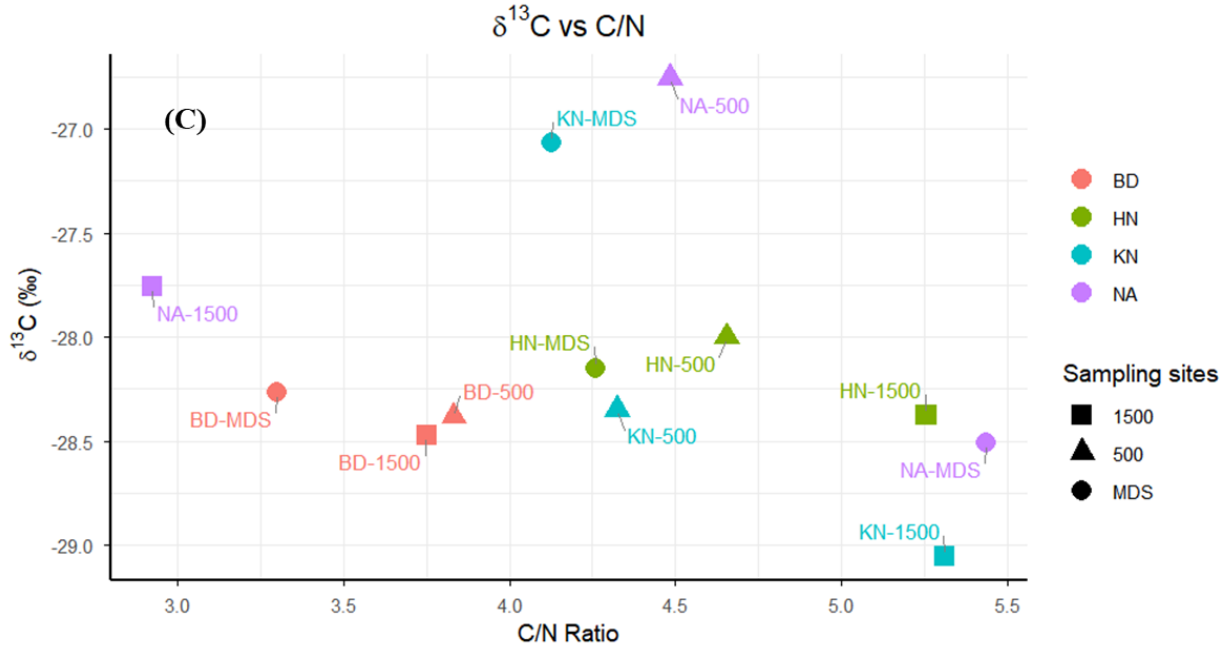

Figure 2. Relationship between Particulate Organic Carbon (POC %) and Particulate Nitrogen (PN %) relative to C/N ratio contours (A), dual isotope plot of $\delta^{13}C$ and δ15N signatures (B) and $\delta^{13}C$ versus C/N ratio in particulate organic matter (C)

3.3 Biochemical and biomolecular composition of POM

3.3.1 Concentrations of carbohydrates, proteins, and lipids

Particulate carbohydrate (PCHO) and proteins (PPRT) concentrations showed a decreasing trend from MDS (PCHO: 55.7 to 109.7 µg L^{-1}; PRT: 56.7 to 145.5 µg L^{-1}) to Adj-W (PCHO: 46.2 to 84.6 µg L^{-1}; PPRT: 32.1 to 94.4 µg L^{-1}) for all stations (Table 2). Unlike PCHO and PPRT, particulate lipids (PLIP) concentrations showed an increasing trend from MDS to Adj-W for NA (59.6 µg L^{-1} to 106.7 µg L^{-1}) and KN (51.6 µg L^{-1} to 70.9 µg L^{-1}), and a decreasing trend for BD (122.7 µg L^{-1} to 83.3 µg L^{-1}). For HN stations, HN_500 (118.1 µg L^{-1}) showed the highest PLIP concentrations, followed by HN_MDS (77.8 µg L^{-1}) and HN_1500 (47.5 µg L^{-1}). Among stations,

BD stations showed the highest average PCHO (90.7 μg L^{-1}), PPRT (105.4 μg L^{-1}), and PLIP (105.4 μg L^{-1}) concentrations.

Table 2. Concentrations of particulate biochemical components, including carbohydrates (P-CHO), proteins (P-PRT), and lipids (P-LIP), alongside their biopolymeric carbon equivalents (BPC-CHO, BPC-PRT, BPC-LIP) and total biopolymeric carbon (BPC) across the sampling stations.

Station	P-CHO (μg L^{-1})	P-PRT (μg L^{-1})	P-LIP (μg L^{-1})	BPC-CHO (μg L^{-1})	BPC-PRT (μg L^{-1})	BPC-LIP (μg L^{-1})	BPC (%)	BPC/POC (%)	Labile (%)
NA_MDS	67.7	61.1	59.6	27.1	29.9	44.7	31.7	31.7	17.8
NA_500	54.9	45.5	67.7	22.0	22.3	50.8	45.1	45.1	21.0
NA_1500	46.2	32.1	106.7	18.5	15.7	80.0	60.0	60.0	18.0
BD_MDS	109.7	145.5	122.7	43.9	71.3	92.0	46.3	46.3	25.7
BD_500	84.6	94.4	110.3	33.8	46.3	82.7	40.0	40.0	19.7
BD_1500	77.8	64.2	83.3	31.1	31.5	62.4	47.7	47.7	23.9
KN_MDS	55.7	56.7	51.6	22.3	27.8	38.7	42.2	42.2	23.8
KN_500	46.8	42.6	51.9	18.7	20.9	38.9	46.9	46.9	23.7
KN_1500	53.4	39.1	70.9	21.4	19.2	53.1	50.1	50.1	21.7
HN_MDS	78.6	97.0	77.8	31.4	47.5	58.3	43.4	43.4	25.0
HN_500	75.3	86.2	118.1	30.1	42.2	88.6	49.5	49.5	22.2
HN_1500	73.7	81.8	47.5	29.5	40.1	35.6	33.5	33.5	22.2

BPC_CHO: Biopolymeric carbon equivalent carbohydrate; BPC_PRT: Carbon equivalent biopolymeric protein; BPC_LIP: Carbon equivalent biopolymeric lipid

3.3.2 Biopolymeric vs. Non-Biopolymeric Carbon in POM

A consistent increase in BPC (%) from MDS to Adj-W was observed at NA and KN (Table 2 and Table S3). In contrast, BD exhibited lower BPC at BD_500 compared to both BD_MDS and BD_1500 (Table 2). For HN, BPC% was highest at HN_500 compared to HN_MDS and HN_1500. Overall, BPC_CHO and BPC_PPRT, representing labile components of POC, showed a consistent difference of 2-6% between MDS and Adj-W at individual sampling stations. The most significant variation occurred at BD sites, with BD_500 showing 19.6% of labile component contributions, followed by BD_1500 (23.9%) and BD_MDS (25.7%).

3.3.3 Monosaccharide composition of POM

Total monosaccharide concentrations at NA and BD declined from MDS to Adj-W (Fig. 3A and Table S3). In contrast, KN and HN exhibited increasing monosaccharide concentrations from MDS to Adj-W. Glucose (8.6 - 47.5 μg L^{-1}) and galactose (3.4 - 9.6 μg L^{-1}) dominated the monosaccharide pool and followed trends similar to total monosaccharides from MDS to Adj-W across stations. Station-wise, average monosaccharide concentrations were highest at BD (59.2 μg L^{-1}), followed by HN (47.9 μg L^{-1}), NA (32.0 μg L^{-1}), and KN (29.0 μg L^{-1}).

The mol% monosaccharide concentrations showed a consistent pattern across MDS and Adj-W for each station, with minor differences (Fig. 3B). However, BD and KN stations showed different compositions compared to NA and HN stations, mainly due to the contributions of glucosamine and rhamnose. Glucose, the dominant monosaccharide, exhibited a decreasing mol% trend from MDS to Adj-W at the BD station, whereas it showed an increasing mol% trend offshore at the other stations.

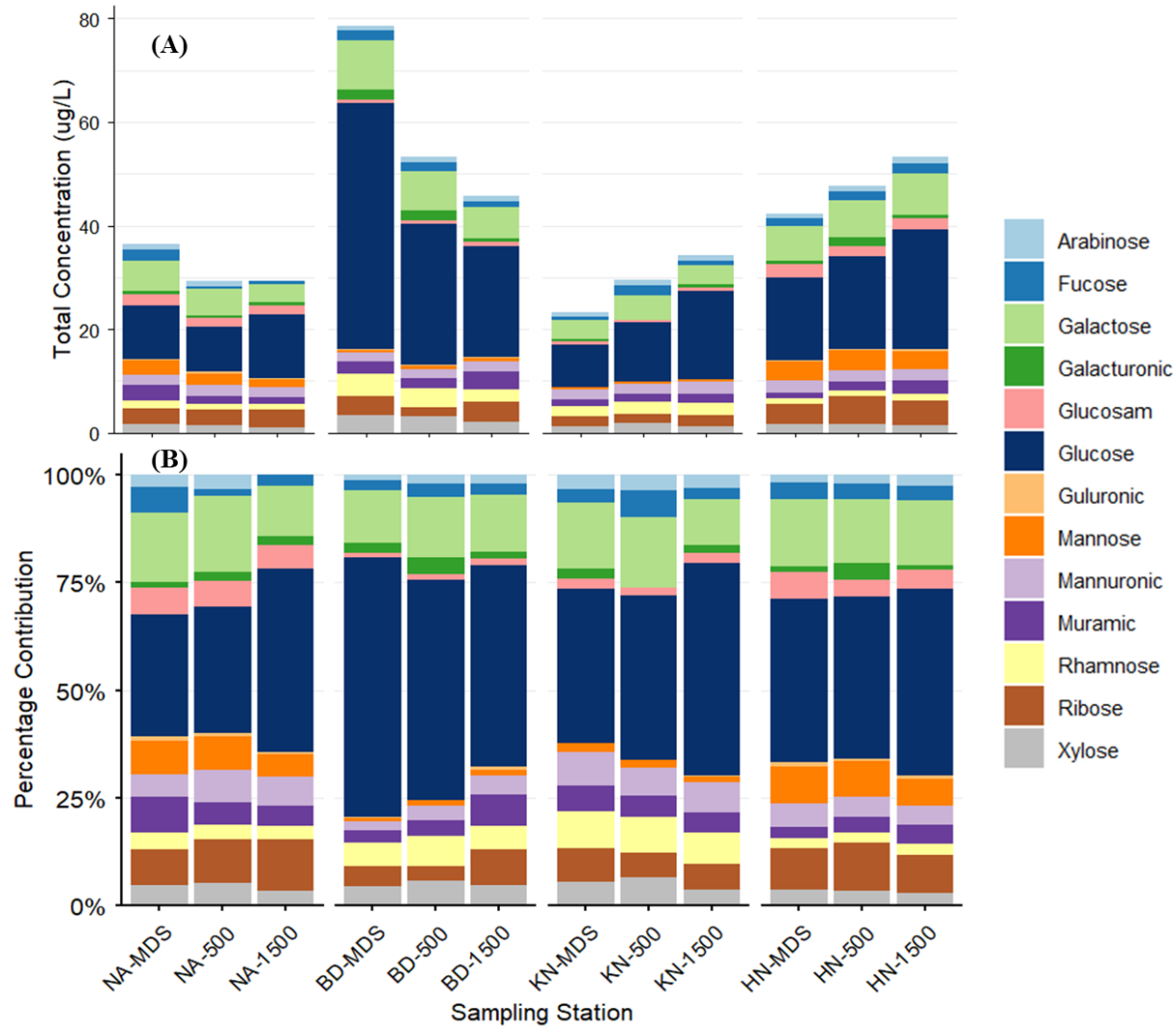

Figure 3. Spatial variation in monosaccharide composition of surface POM across fjord stations. (A) Concentrations (μg L^{-1}) and (B) relative percentage contributions of individual monosaccharides at macroalgal bed (MDS), 500 m, and 1500 m sites at NA, BD, KN, and HN.

3.3.4 Amino acid composition of POM

A clear decreasing trend in total amino acid concentrations from MDS to Adj-W was observed at BD and KN (Fig. 4A and Table S3). In contrast, concentrations at NA increased from NA_MDS to NA_500 further declined at NA_1500. At HN, total amino acid concentrations decreased

slightly from HN_MDS to HN_500 and then increased at HN_1500. Among stations, the average total amino acid concentrations were highest at BD (113 μg L^{-1}) followed by HN (101.6 μg L^{-1}), NA (61 μg L^{-1}) and KN (33.3 μg L^{-1}). The average concentrations of individual amino acids were also higher in MDS than in Adj-W (Table S4). The BD station showed the highest concentrations of individual amino acids, with Asp (26.1 μg L^{-1}), Glu (29.8 μg L^{-1}), Gly (33.9 μg L^{-1}), Arg (27.6 μg L^{-1}), and Lys (9.4 μg L^{-1}) peaking at the MDS and declining toward Adj-W (Asp: 5.6 μg L^{-1}; Glu: 15.9 μg L^{-1}; Gly: 14.4 μg L^{-1}; Arg: 14.4 μg L^{-1}; Lys: 6.5 μg L^{-1}). A similar decreasing pattern of the individual amino acids was observed for the KN station. Exceptions to the low individual amino acid concentrations at Adj-W (500 and 1500 m locations) included high Gly at NA_500 (33.5 μg L^{-1}), and high Gly (26.7 μg L^{-1}) and Arg (19.1 μg L^{-1}) at HN_1500.

Mol% concentrations of different amino acids indicated that Gly, Glu, and Arg were the dominant contributors across all sampling stations (Fig. 4B). The mol% concentration of Glu showed a decreasing trend from MDS to Adj-W at NA (24.1 % to 13.7%), KN (19.7% to 14.0%) and HN (13.3% to 10.9%) stations, whereas BD showed an increasing trend (MDS: 16.6%; Adj-W: 21.3%). In contrast, Gly and Arg exhibited similar spatial patterns across stations, with Gly showing its highest mol% contribution at the 500 m station at NA, BD, and KN, while Arg displayed a consistent increase from MDS to Adj-W across these stations.

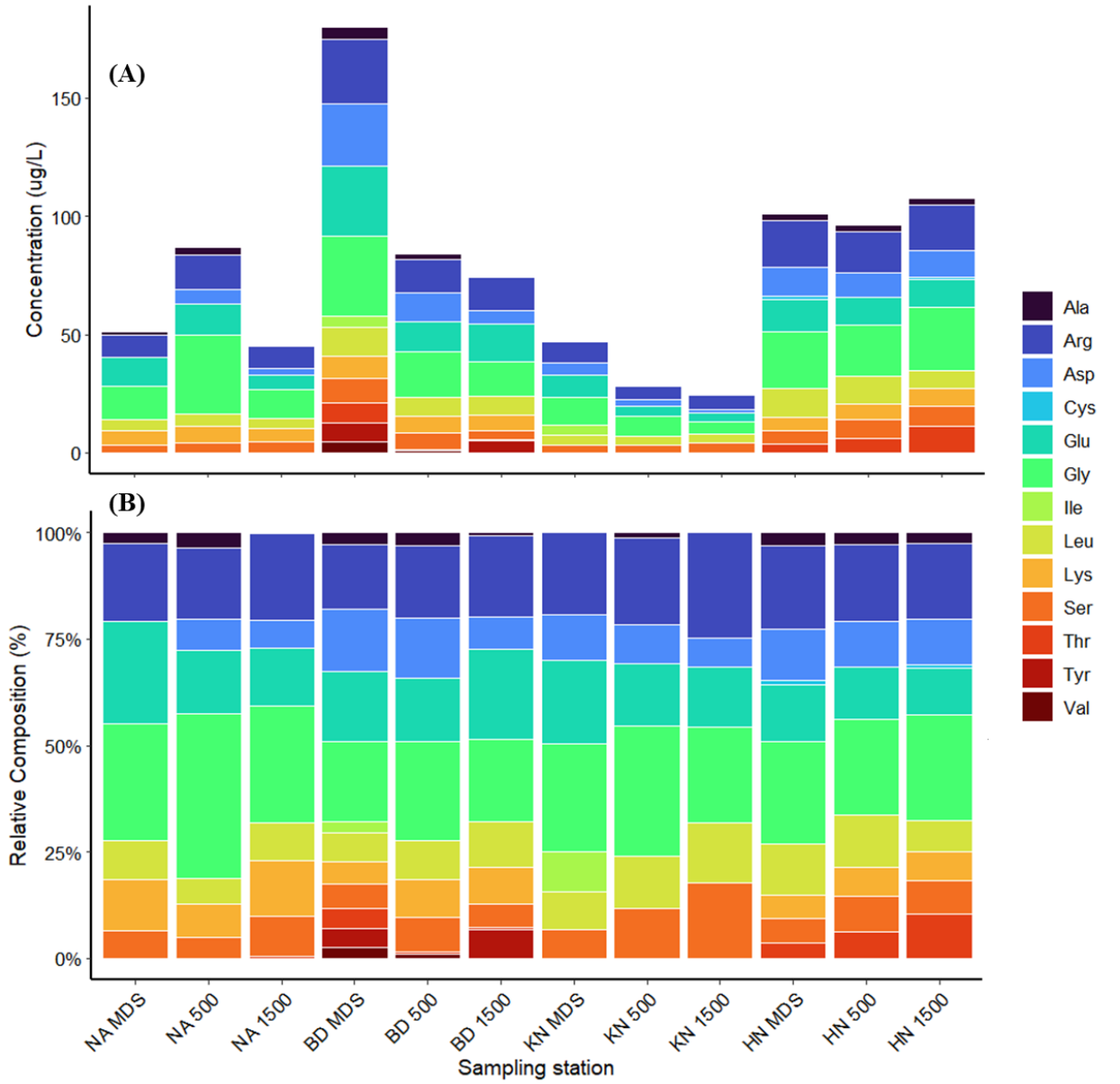

330

331 **Figure 4.** Spatial variation in amino acid composition of surface POM across fjord stations. (A)

332 Concentrations (μg L^{-1}) and (B) relative percentage contributions of individual amino acids at

333 macroalgal beds (MDS), 500 m and 1500 m sites in NA, BD, KN, and HN.

334

335 **3.4 Statistical analysis**

Strong positive correlations were observed between PN and POC, PCHO, and PPRT ($r > 0.83$, $p<0.05$), with an exceptionally high correlation between PPRT and PCHO ($r = 0.96$, $p<0.05$) (Fig. S2A). In contrast, negative correlations were observed between BPC_LIP% and the non-BPC fraction ($r = -0.95$, $p<0.05$), and between nitrate and biochemical parameters (POC, PN, PCHO, PPRT) ($r < -0.66$, $p<0.05$). Despite consistent trends across parameters, ANOVA indicated no significant differences between MDS and Adj-W, suggesting gradual lateral transformations rather than abrupt distance-related changes, together with pronounced spatial heterogeneity among stations (Table S1).

Mannuronic acid (ManA) showed strong negative correlations with POC ($r = -0.79$) and PCHO ($r = -0.92$) (Fig. S2B). Glucose and galactose were negatively correlated with several compounds, including glucosamine ($r = -0.72$), mannose ($r = -0.70$), ribose ($r = -0.59$), and ManA ($r = -0.63$). Rhamnose exhibited pronounced negative relationships with guluronic acid (GulA; $r = -0.83$), glucosamine ($r = -0.76$), mannose ($r = -0.85$), and ribose ($r = -0.73$), whereas galactose was positively correlated with fructose ($r = 0.61$) and arabinose ($r = 0.58$). Strong positive associations were also observed among mannose, glucosamine ($r = 0.91$), and ribose ($r = 0.76$), with ribose additionally correlating positively with glucosamine ($r = 0.79$).

In PCA, the first two principal components explained 49.0% of the total variance, with PC1 and PC2 accounting for 30.1% and 18.9%, respectively (Fig. 5). PC1 was positively loaded by POC, PN, PCHO, PPRT, glucose, galactose, and labile amino acids (Asp, Glu, Thr), whereas negative PC1 loadings were associated with muramic acid, arabinose, fucose, and inorganic nutrients. Sample scores showed a spatial organization, with MDS plotting toward positive PC1 values and Adj-W progressively shifting toward negative PC1 values, which was seen more prominently for BD stations.

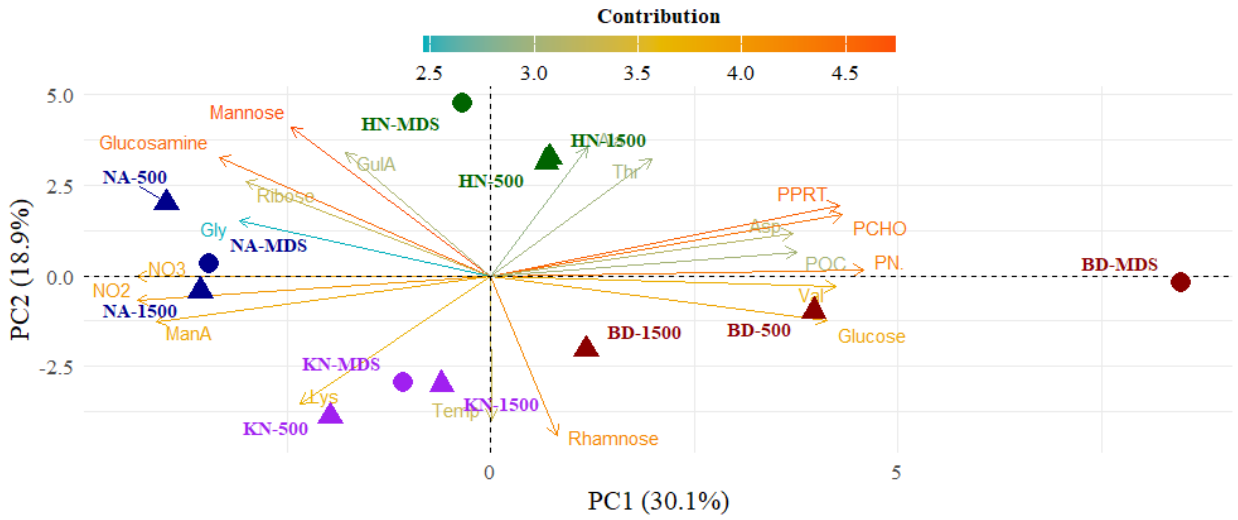

Figure 5. Principal Component Analysis (PCA) biplot of biogeochemical variables across different sample sites. The first two principal components (PC1 and PC2) account for 30.1% and 18.9% of the total variance, respectively. Individual samples are represented by colored shapes, categorized by site (e.g., NA, HN, KN, BD) and location (e.g., MDS, 500, 1500). Vectors (arrows) indicate the loadings of specific variables, including carbohydrates (e.g., Mannose, Glucose, Rhamnose), nutrients (NO^{2-}, NO^{3-}), and organic matter indicators (POC, PN, PCHO, PPRT). The color scale of the vectors represents the contribution of each variable to the principal components.

4. Discussion

The present study provides a multi-proxy assessment of POM in the surface waters of macroalgal beds in Kongsfjorden, integrating bulk biochemical, isotopic, biopolymeric composition, and molecular biomarkers. Elevated bulk (POC, PN, PCHO, and PPRT) and molecular (monosaccharides and amino acids) concentrations at MDS indicated that macroalgal beds act as localized sources of biochemically labile organic matter. The results demonstrated that macroalgal beds imprint surface waters with distinct biochemical and molecular signatures that are

redistributed across fjord-scale gradients. The PCA demonstrates that macroalgae influence surface POM along a continuous multivariate gradient rather than discrete habitat classes. The systematic offshore decline of these compounds, together with internal reorganization of the biopolymeric and molecular composition, shows that macroalgal-derived POM is efficiently exported and selectively transformed during lateral transport (Fig. 6).

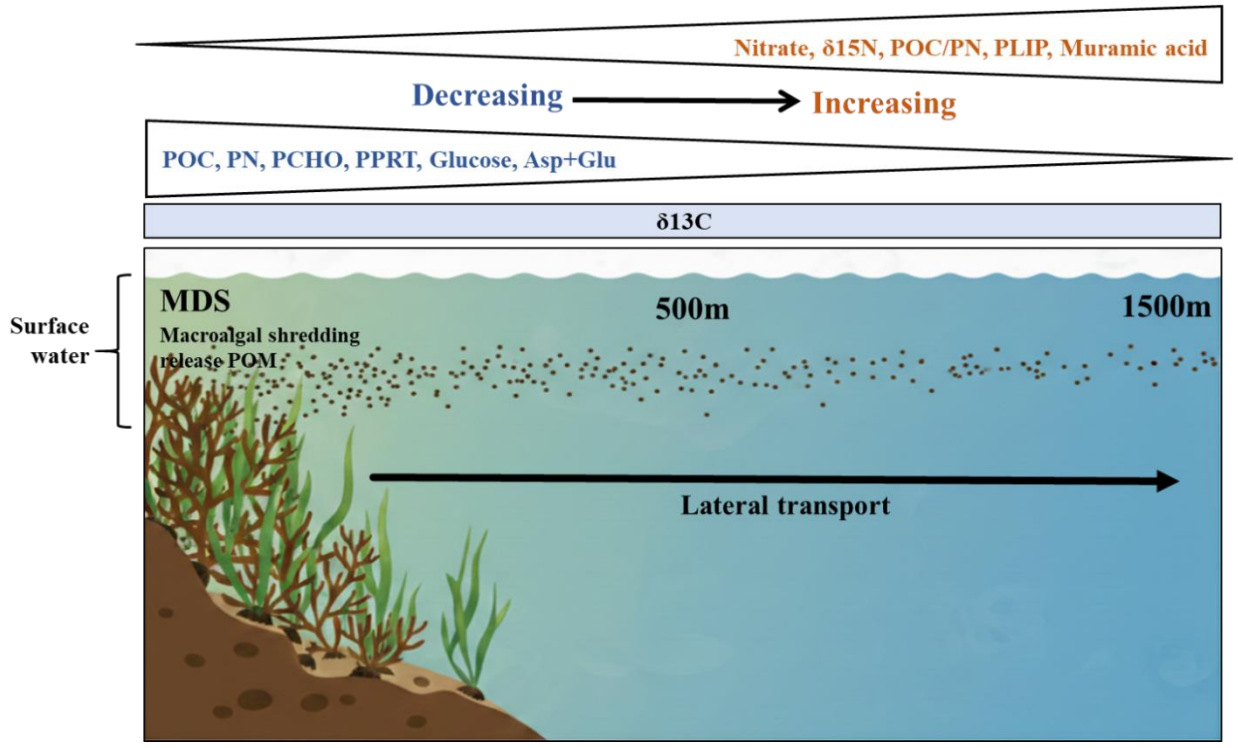

Figure 6. Schematic showing the biochemical nature of POM at macroalgal-dominated sites and its transformation during lateral transport.

4.1 Influence of Macroalgal Beds on Surface POM Biochemical Composition

Macroalgal beds produce substantial organic carbon via photosynthesis, which enters surrounding waters (Chen et al., 2020; Filbee-Dexter et al., 2022; Pessarrodona et al., 2022; Watanabe et al., 2020). The observed higher concentrations of POC and PN at MDS relative to Adj-W, together

with consistently higher PCHO and PPRT, indicates localized enrichment of particulate matter near macroalgal beds. The inverse relationship between nitrate and POC, PN, PCHO, and PPRT ($r = -0.82$, $p < 0.05$) reflects biological assimilation of dissolved nutrients into the particulate pool, reinforcing the role of active coastal production in shaping POM composition along the fjord gradient. Macroalgal tissues are structurally rich in polysaccharides and contain substantial protein fractions, and the release of tissue fragments, sloughed material, and epiphyte-associated biomass (Kennedy and Blain, 2025; Watanabe et al., 2020) provides a direct pathway for incorporation of macroalgal carbon into surface POM contributing to Arctic coastal carbon cycling (Ager et al., 2023). Strong positive correlations ($r > 0.83$, $p < 0.05$) between PN and POC, PCHO, and PPRT indicate tightly coupled carbon and nitrogen incorporation during fresh organic matter production. The remarkably strong positive correlation between PPRT and PCHO ($r = 0.96$, $p < 0.05$) further indicates tightly coupled biological production and POM synthesis in macroalgal beds. The multivariate analysis of POM as resolved by PCA showed PC1 (30.1% variance) was dominated by PCHO, PPRT, PN, POC, glucose, and Asp and separated MDS from Adj-W along a continuous biochemical gradient, especially prominent for BD station (Fig. 5). The strong positive loadings of labile carbon and nitrogen compounds supported a distinct organic-rich biochemical state of surface POM at MDS.

Although macroalgal biomass and detritus are generally carbon-rich, three of the four stations (BD, KN, and HN) exhibited lower POC/PN ratios at the MDS sites than Adj-W. This pattern likely reflects contributions from fresh, nitrogen-rich organic matter produced within macroalgal habitats, possibly including phytoplankton, epiphytic microalgae, and benthic primary producers associated with kelp beds (Burfeid-Castellanos et al., 2021; Stanca and Parsons, 2021), which could be re-suspended into surface waters and become part of POM. Kelp forest POM

characteristics are highly variable depending on the water column conditions, which also influence contributions from macroalgal detritus and other autochthonous primary producers (Dyer et al., 2019). In favorable conditions, other primary producers may outweigh the stoichiometric signal of macroalgal tissue itself, resulting in relatively low POC/PN ratios of POM near macroalgal beds (Chen et al., 2020). Similarly, heterotrophic bacteria are typically richer in nitrogen and phosphorus than phytoplankton, and their colonization of particles can lower the bulk POC/PN ratio by contributing nitrogen-rich biomass (Jo et al., 2021). The subsequent increase in POC/PN ratios from MDS to Adj-W is consistent with preferential microbial degradation of labile nitrogen-rich compounds during lateral transport (Vidal et al., 2018), leading to relative enrichment of carbon-rich material with distance from source habitats.

$\delta^{13}C$ values of POM are widely used to trace organic matter sources (Gao et al., 2008; Pineault et al., 2013). Most macroalgae typically exhibit $\delta^{13}C$ values between −34.6‰ to −2.2‰ (Velázquez-Ochoa et al., 2022), though some brown macroalgal species show more negative signatures, ranging from −20‰ to −35‰ (Fredriksen, 2003). In Arctic coastal systems, marine phytoplankton-derived organic matter typically exhibits $\delta^{13}C$ values between −20‰ and −26‰, whereas terrestrial organic matter derived from C3 vegetation is generally more depleted, around −26‰ to −29‰ (Gao et al., 2008; Pineault et al., 2013). However, substantial overlap between marine and terrestrial isotopic ranges complicates source discrimination in Arctic fjord systems (Kumar et al., 2016; Singh et al., 2024b). The similarity of $\delta^{13}C$ values between MDS and Adj-W indicates that macroalgal material does not dominate bulk POM isotopically; instead, it contributes substantially within a mixed particulate pool of macroalgal, phytoplanktonic, and terrestrial organic matter in Arctic fjords (Ørberg et al., 2023; Roy et al., 2025). This muted isotopic signal likely reflects that macroalgal influence on surface POM is not solely derived from detached kelp

tissue, but is also mediated by contributions from epiphytic and benthic microalgal production (Burfeid-Castellanos et al., 2021; Stanca and Parsons, 2021) and biochemically distinct macroalgal fractions, whose $\delta^{13}C$ values overlap those of pelagic organic matter.

$\delta^{15}N$ values of POM exceeding ~2‰ as observed in this study are consistent with marine nitrate-based production and microbial reworking, rather than atmospheric or N_2-fixation sources (Kuzyk et al., 2010), where intense benthic–pelagic coupling and rapid recycling of dissolved inorganic nitrogen promote isotopic enrichment of the available nitrogen pool (Elliott Smith and Fox, 2022). Reflecting the pattern more prominently, $\delta^{15}N$ value at BD_MDS (5.0‰), which was already high, further increased toward Adj-W (BD_500: 12.5‰, BD_1500: 15.9‰), indicating relatively fresher marine-derived organic matter within the macroalgal beds, which is transformed into relatively higher trophic contributions in surrounding waters.

4.2 Transformation of surface POM during lateral transport from macroalgal beds to adjacent waters

The biochemical composition of POM provides valuable insights into the nature of organic carbon and its benthic-pelagic coupling in macroalgal beds (Elliott Smith and Fox, 2022; Renaud et al., 2015). The observed systematic offshore changes in POM composition revealed both lateral transport and early transformation of macroalgal beds derived particles across the fjord (Vidal et al., 2018). The concentrations of PCHO and PPRT declined consistently from MDS to Adj-W, indicating progressive dilution of organic matter with distance sourced from macroalgal beds and associated autochthonous production (Ørberg et al., 2023; Smale et al., 2022; Simpkins et al., 2025). These labile compounds are preferentially consumed by particle-associated and free-living microbes (Jain et al., 2019), serving as indicators of freshly produced, easily degradable organic

matter (Li et al., 2025). In contrast, PLIP generally increased offshore (except at BD), indicating a relative enrichment of lipid-rich pelagic material and/or the preferential preservation of more stable lipid compounds during transport. This pattern likely reflects selective microbial degradation of labile carbohydrates and proteins during lateral transport, combined with mixing with newly produced pelagic material (Li et al., 2025), highlighting dynamic compositional transformation of POM from MDS to Adj-W.

The compositional shift in POM was further supported by changes observed in BPC fractions. BPC represents the labile fraction of POM, mainly comprising proteins, carbohydrates, and a lipid fraction, whereas the non-BPC fraction includes more refractory components such as lignin, humic substances, black carbon, and cellulose (Fabiano et al., 1993; Lobbes et al., 2000; Tselepides et al., 2000). Among BPC constituents, %BPC_lipid increased markedly from MDS (17.8 ± 2.8%) to Adj-W (25.1 ± 8.6%), whereas the labile fraction (proteins and carbohydrates) showed minor differences between MDS (23.1 ± 3.6%) and Adj-W (21.5 ± 2.5%). This pattern suggests a relative enrichment of more stable organic matter within POC, accompanied by lateral degradation of labile components, consistent with the observed decline in POC from MDS to Adj-W. Further, the strong inverse relationship between %BPC_LIP and the non-BPC fraction ($r = -0.95$, $p < 0.05$) suggested biochemical reorganization of POM during lateral transport, consistent with selective degradation and compositional restructuring rather than just uniform bulk loss. In support, PCA also showed a progressive leftward shift from MDS to Adj-W along PC1 (Fig. 5) demonstrating lateral export of POM from macroalgal beds to surrounding waters as a gradient, consistent with progressive dilution and selective transformation during fjord-scale transport of POM.

4.3 Molecular-level evidence for macroalgal imprint and early transformation of POM

Molecular fingerprints based on monosaccharides and amino acids offer direct insight into the origin, bioavailability, and early diagenetic transformation of organic matter (Grosse et al., 2021; Jo et al., 2022). Glucose is a common constituent of the macroalgal storage polysaccharide laminarin, while fucose, galactose, and uronic acids (glucuronic, mannuronic, and guluronic acids) are key monomers of structural polysaccharides such as alginates and fucans (Singh et al., 2024a). This carbohydrate pool of macroalgae is bound within structurally complex cell-wall polymers that are relatively resistant to microbial degradation (Kennedy and Blain, 2025). In contrast, phytoplankton cell walls and extracellular matrices are dominated by cellulose, and species-specific storage glucans, which are recycled relatively rapidly in surface waters (Biersmith and Benner, 1998). Glucose and galactose were observed to be the dominant monosaccharides throughout the samples, reflecting a shared baseline of organic matter likely derived from a mixture of macroalgal detritus, phytoplankton, and bacterial biomass (Li et al., 2025; Smale et al., 2022). However, the positive correlation of glucose with POC and PCHO indicated a relative enrichment of a labile, carbohydrate-rich organic matter pool at MDS where POC and PCHO were higher than Adj-W. On the other hand, the negative correlation between glucose and other monosaccharides such as galactose, mannose, mannuronic acid, ribose, and glucosamine reflected a relative increase in structurally complex, algal, microbial, and zooplankton-associated sugars during lateral transport and early diagenesis.

Amino acid distributions provide complementary evidence for POM source and lability patterns, as their composition reflects both the origin and degree of degradation (Grosse et al., 2021; Jo et al., 2022). The total amino acid concentrations observed in this study (24–180 $\mu g\ L^{-1}$) fall within the reported values from coastal Kongsfjorden (Zhu et al., 2016) and across Fram-Strait

(Grosse et al., 2021). The average total amino acids were higher at MDS (94.8 μg L^{-1}) than at Adj-W (68.4 μg L^{-1}), with BD exhibiting the highest average concentration (113.0 μg L^{-1}), indicating fresher, nitrogen-rich, proteinaceous POM in surface waters, along with elevated PPRT and low C:N ratios observed near macroalgal beds. At BD and KN, total amino acids drop by ~60–50% from MDS to Adj-W, indicating preferential microbial utilization of proteinaceous, nitrogen-rich matter during lateral transport, consistent with the observed offshore increase in POC/PN and PLIP enrichment. NA and HN show mid-station or distal increases (NA_500, HN_1500), likely reflecting local resuspension or secondary production, supporting spatial heterogeneity as discussed before. The combined Asp + Glu content, reflecting the freshness of organic matter and the diagnostic Asp/Gly ratio, indicates the degradation state of organic matter (Machado et al., 2020; Yao et al., 2023). The decline in Glu, Asp, and Asp/Gly ratio, and the relative enrichment of Gly and Arg from MDS to Adj-W for most of the stations further provide molecular signatures for early-stage protein degradation and microbial reworking of macroalgal-derived POM during lateral transport.

Together, the coupled behavior of carbohydrates and amino acids demonstrated that macroalgal beds imprint surface POM with a distinct molecular signature that is progressively modified during fjord-scale export. These molecular patterns corroborate the bulk biochemical and isotopic evidence, indicating that macroalgal-derived organic matter is redistributed across coastal gradients while undergoing selective early transformation. The pronounced total monosaccharides and amino acid enrichment at BD (especially BD_MDS), which also exhibited the highest POC and PPRT concentrations, identifies this site as a biogeochemical hotspot of macroalgal influence, reinforcing the spatial coherence of macroalgal signatures across independent biochemical proxies.

4.4 Brandal (BD) as a biogeochemical hotspot of macroalgal influence in Kongsfjorden

BD station, among all studied stations, consistently emerged as an organic-rich site, showing characteristics of macroalgal-influenced surface POM, highlighting its role as a biogeochemical hotspot within Kongsfjorden. With the highest concentrations of POC, PN, PCHO, PPRT, total monosaccharides, and total amino acids, the BD station contributed the most in the PCA biplot (Fig. 5), which demonstrated local production and accumulation of biochemically labile organic matter within this macroalgal-dominated habitat. The strong gradient observed across PN, $\delta^{15}N$, C:N, PPRT, and amino acid composition from MDS to Adj-W at BD indicated nitrogen assimilation, dominance of fresh marine organic matter in macroalgal bed, and their progressive downstream alteration. At the molecular level as well, BD_MDS was strongly enriched in glucose and other macroalgal sugars (fucose, galactose, mannuronic acid), with total monosaccharides and glucose declining offshore. Similarly, the offshore decrease in labile amino acids (e.g., Asp, Glu) provides a molecular signature for early degradation during export, indicating that the BD macroalgal bed is a major source of biochemically active POM and a key contributor to fjord-scale redistribution (Van der Mheen et al., 2024).

Situated on the westernmost part of the south shore, BD is influenced by Atlantic water inflow, which creates relatively warmer and more saline conditions (Williams, 2017; Wilson, 2022; Woelfel et al., 2014), supporting abundant micro-phytobenthic and benthic mosses (Woelfel et al., 2014). At BD, macroalgal cover is not higher than at other sites, yet detritus accumulation is substantial, supporting elevated benthic faunal diversity. The presence of a deep trench, combined with storm-driven transport, concentrates detritus at BD (Schimani Katherina, 2019). Habitat heterogeneity further drives microbial community assembly and functional differentiation (Huang et al., 2026), reflected in high macroalgal detrital cover and meiofaunal density (Schimani

et al., 2022). Additionally, BD exhibits significantly lower turbidity than glacier-proximal sites, which prevents mineral masking of organic signatures and provides a stable light regime for primary producers (Bianchi et al., 2020). Collectively, these features make BD a retention zone for macroalgal detritus, acting as a biogeochemical hotspot and a critical repository for macroalgal-derived carbon. While Brandal represents a biogeochemical hotspot, its broader representativeness is constrained due to spatial variability in macroalgal structure and function across high Arctic fjords, driven by variation in latitude, ice scour, light availability, terrestrial runoff, and glacier-induced salinity and turbidity gradients (Bartsch et al., 2016). Thus, although Brandal provides a high-resolution case study, caution is required when extrapolating its biogeochemical fluxes to fjords characterized by intense glacial runoff, seasonal sea-ice cover, and a different community composition.

4.5 Implications of macroalgal-beds for Arctic coastal carbon cycling

Unlike previous studies on POM in Kongsfjorden that primarily used bulk isotopes (e.g., $\delta^{13}C$, $\delta^{15}N$) and their ratios for source apportionment (Kuliński et al., 2014; Singh et al., 2024b), our study advances the biochemical perspective by integrating molecular level biomarkers (amino acids, sugars) with a spatially resolved transect. This approach shifts the focus from POM origin to its functional quality, enabling differentiation between labile and refractory pools. Our study demonstrates that macroalgal-dominated sites in Kongsfjorden act as hotspots of labile and bioavailable organic matter, significantly shaping the composition and lability of POM in adjacent waters. The intermediate and variable patterns observed at the few stations highlight that the influence of MDS was not uniform but forms a gradient shaped by local hydrodynamics, freshwater inputs, and nutrient availability. The strong spatial heterogeneity observed, particularly

the emergence of Brandal as a biogeochemical hotspot, emphasizes that macroalgal impacts on coastal carbon cycling are unevenly distributed within fjord systems. Such localized but persistent sources of organic carbon from macroalgal beds to surrounding waters, thereby dampening the seasonal variability in carbon availability (Norkko et al., 2007), enhancing benthic-pelagic food-web stability and increase ecosystem resilience to inter-annual fluctuations in pelagic primary production (Norkko et al., 2007; Renaud et al., 2015).

Although our study focused on surface waters, future research should include vertical fluxes of POM near macroalgal beds and their coupling to hydrodynamics. Additionally, the effects of seasonal variability driven by glacial melt, riverine runoff, and episodic nutrient inputs at the coast are important because they can alter carbon concentrations and biochemical composition, particularly in nearshore macroalgal habitats (Ager et al., 2023). Experimental studies at model sites like BD could further help elucidate the rates of labile carbon turnover, microbial utilization, and nutrient remineralization at these sites. As macroalgal habitats are expanding under ongoing warming, resolving the contribution of macroalgal biomass and beds-associated organic matter dynamics in coastal biogeochemistry would be important for estimating Arctic carbon budgets and ecosystem functioning.

Conclusion

The present study provides new insights into the role of Arctic macroalgal beds as active drivers of coastal particulate organic matter dynamics in Kongsfjorden, an Arctic fjord. By integrating bulk biogeochemical composition, stable isotopes, biopolymeric composition, and molecular biomarkers, we demonstrate that macroalgal habitats imprint surface waters with a distinct biochemical and molecular signature. Elevated concentrations of POC, PN, carbohydrates,

proteins, monosaccharides, and amino acids at macroalgal-dominated sites indicate that macroalgal beds act as localized sources of biochemically labile organic matter to the overlying water column. Systematic offshore declines in bulk parameters, together with internal reorganization of biopolymeric and molecular composition, reveal that macroalgal-beds derived POM is efficiently exported across fjord-scale gradients and undergoes selective early-stage transformation during lateral transport. The muted bulk isotopic gradients further indicate that macroalgal influence is expressed through continuous mixing and biochemical restructuring of a heterogeneous particulate pool rather than simple replacement of pelagic organic matter. A pronounced spatial gradient was observed across the stations, within which Brandal emerged as a distinct biogeochemical hotspot of macroalgal-associated organic matter dynamics, as supported by our multiproxy study. Overall, our findings show that macroalgal beds function as dynamic benthic–pelagic coupling zones that redistribute and transform organic carbon beyond their immediate habitat. As macroalgal cover continues to expand along Arctic coastlines under climate warming, their contribution to coastal carbon fluxes is likely to intensify, with important implications for Arctic carbon budgets and ecosystem functioning.

Data availability. The data are available in the Zenodo repository at: https://doi.org/10.5281/zenodo.18457176 (Jagtap et al., 2026).

Author contributions. ASJ and AS conceptualized the study with input from AJ. AS and AJ conducted the fieldwork, while laboratory analyses were performed by ASJ and NR. MT analyzed the elemental and isotopic data. All authors were involved in the interpretation of the results, the revision, and the writing of the final version of the paper.

Competing interests. The corresponding author has declared that none of the authors has any competing interests.

Acknowledgement. We extend our gratitude to the Director of the National Centre for Polar and Ocean Research for their support in this work. We acknowledge funding from the Ministry of Earth Sciences. We are thankful to Dr. Biswajit Roy, Dr. PV Bhaskar and Ms. Viola Rodrigues for sampling assistance, nutrient and EA-IRMS analysis, respectively.

Financial Support. This research was funded by the National Centre for Polar and Ocean Research (NCPOR), Ministry of Earth Sciences (MoES), India.

References

Ager, T. G., Krause-Jensen, D., Olesen, B., Carlson, D. F., Winding, M. H. S., and Sejr, M. K.: Macroalgal habitats support a sustained flux of floating biomass but limited carbon export beyond a Greenland fjord, Sci. Total Environ., 872, 162224, https://doi.org/10.1016/j.scitotenv.2023.162224, 2023.

Assis, J., Serrão, E. A., Duarte, C. M., Fragkopoulou, E., and Krause-Jensen, D.: Major Expansion of Marine Forests in a Warmer Arctic, Front. Mar. Sci., 9, 1–10, https://doi.org/10.3389/fmars.2022.850368, 2022.

Bartsch, I., Paar, M., Fredriksen, S., Schwanitz, M., Daniel, C., Hop, H., and Wiencke, C.: Changes in kelp forest biomass and depth distribution in Kongsfjorden, Svalbard, between 1996–1998 and 2012–2014 reflect Arctic warming, Polar Biol., 39, 2021–2036,

https://doi.org/10.1007/s00300-015-1870-1, 2016.

Bianchi, T. S., Arndt, S., Austin, W. E. N., Benn, D. I., Bertrand, S., Cui, X., Faust, J. C., Koziorowska-makuch, K., Moy, C. M., Savage, C., Smeaton, C., Smith, R. W., and Syvitski, J.: Earth-Science Reviews Fjords as Aquatic Critical Zones (ACZs), Earth-Science Rev., 203, 103145, https://doi.org/10.1016/j.earscirev.2020.103145, 2020.

Biersmith, A. and Benner, R.: Carbohydrates in phytoplankton and freshly produced dissolved organic matter, Mar. Chem., 63, 131–144, https://doi.org/10.1016/S0304-4203(98)00057-7, 1998.

Buchholz, C. M. and Wiencke, C.: Working on a baseline for the Kongsfjorden food web: production and properties of macroalgal particulate organic matter (POM), Polar Biol., 39, 2053–2064, https://doi.org/10.1007/s00300-015-1828-3, 2016.

Burfeid-Castellanos, A. M., Martín-Martín, R. P., Kloster, M., Angulo-Preckler, C., Avila, C., and Beszteri, B.: Epiphytic diatom community structure and richness is determined by macroalgal host and location in the South Shetland Islands (Antarctica), PLoS One, 16, 1–21, https://doi.org/10.1371/journal.pone.0250629, 2021.

Carlson, D. F., Suzuki, N., Carrasco, R., Filbee-Dexter, K., Gillard, L. C., Myers, P. G., Queirós, A. M., Assis, J., Duarte, C. M., Sejr, M., and Krause-Jensen, D.: Ocean transport and vertical mixing connect Greenland's macroalgae to deep ocean carbon sinks, Sci. Total Environ., 1012, https://doi.org/10.1016/j.scitotenv.2025.181247, 2026.

Castro de la Guardia, L., Bartsch, I., Hop, H., Niedzwiedz, S., Düsedau, L., Diehl, N., Krause-Jensen, D., Sejr, M., Ager, T. G., Gattuso, J. P., Schlegel, R. W., Miller, C. A., Filbee-Dexter, K., and Duarte, P.: Predicting potential Arctic kelp distribution and lower-depth biomass from seafloor irradiance, Limnol. Oceanogr. Methods, https://doi.org/10.1002/lom3.70018, 2025.

664 Chen, S., Xu, K., Ji, D., Wang, W., Xu, Y., Chen, C., and Xie, C.: Release of dissolved and
665 particulate organic matter by marine macroalgae and its biogeochemical implications, Algal
666 Res., 52, 102096, https://doi.org/10.1016/j.algal.2020.102096, 2020.
667 Dai, A., Luo, D., Song, M., and Liu, J.: Arctic amplification is caused by sea-ice loss under
668 increasing CO 2, Nat. Commun., 10, 1–13, https://doi.org/10.1038/s41467-018-07954-9, 2019.
669 Danovaro, R., Dell'Anno, A., and Fabiano, M.: Bioavailability of organic matter in the
670 sediments of the Porcupine Abyssal Plain, northeastern Atlantic, Mar. Ecol. Prog. Ser., 220, 25–
671 32, https://doi.org/10.3354/meps220025, 2001.
672 Duarte, C. M., Losada, I. J., Hendriks, I. E., Mazarrasa, I., and Marbà, N.: The role of coastal
673 plant communities for climate change mitigation and adaptation, Nat. Clim. Chang., 3, 961–968,
674 https://doi.org/10.1038/nclimate1970, 2013.
675 Dubois, M., Gilles, K. A., Hamilton, J. K., Rebers, P. A., and Smith, F.: Colorimetric Method for
676 Determination of Sugars and Related Substances, 350–356, 1956.
677 Düsedau, L., Fredriksen, S., Brand, M., Fischer, P., Karsten, U., Bischof, K., Savoie, A., and
678 Bartsch, I.: Kelp forest community structure and demography in Kongsfjorden (Svalbard) across
679 25 years of Arctic warming, Ecol. Evol., 14, 1–25, https://doi.org/10.1002/ece3.11606, 2024.
680 Dyer, D. C., Butler, M. J., Smit, A. J., Anderson, R. J., and Bolton, J. J.: Kelp forest POM during
681 upwelling and downwelling conditions: Using stable isotopes to differentiate between detritus
682 and phytoplankton, Mar. Ecol. Prog. Ser., 619, 17–34, https://doi.org/10.3354/meps12941, 2019.
683 Elliott Smith, E. A. and Fox, M. D.: Characterizing energy flow in kelp forest food webs: a
684 geochemical review and call for additional research, Ecography (Cop.)., 2022, 1–16,
685 https://doi.org/10.1111/ecog.05566, 2022.
686 Fabiano, M., Povero, P., and Danovaro, R.: Distribution and composition of particulate organic

matter in the Ross Sea (Antarctica), Polar Biol., 13, 525–533, https://doi.org/10.1007/BF00236394, 1993.

Filbee-Dexter, K. and Wernberg, T.: Substantial blue carbon in overlooked Australian kelp forests, Sci. Rep., 10, 1–6, https://doi.org/10.1038/s41598-020-69258-7, 2020.

Filbee-Dexter, K., MacGregor, K. A., Lavoie, C., Garrido, I., Goldsmit, J., Castro de la Guardia, L., Howland, K. L., Johnson, L. E., Konar, B., McKindsey, C. W., Mundy, C. J., Schlegel, R. W., and Archambault, P.: Sea Ice and Substratum Shape Extensive Kelp Forests in the Canadian Arctic, Front. Mar. Sci., 9, 1–27, https://doi.org/10.3389/fmars.2022.754074, 2022.

FOLCH, J., LEES, M., and SLOANE STANLEY, G. H.: A simple method for the isolation and purification of total lipides from animal tissues., J. Biol. Chem., 226, 497–509, https://doi.org/10.1016/s0021-9258(18)64849-5, 1957.

Fredriksen, S.: Food web studies in a Norwegian kelp forest based on stable isotope (δ13C and δ15N) analysis, Mar. Ecol. Prog. Ser., 260, 71–81, https://doi.org/10.3354/meps260071, 2003.

Gao, J., Wang, Y., Pan, S., Zhang, R., Li, J., and Bai, F.: Spatial distributions of organic carbon and nitrogen and their isotopic compositions in sediments of the Changjiang Estuary and its adjacent sea area, J. Geogr. Sci., 18, 46–58, https://doi.org/10.1007/s11442-008-0046-0, 2008.

Grasshoff: Methods_Seawater_Analysis, 2009.

Grosse, J., Nöthig, E. M., Torres-Valdés, S., and Engel, A.: Summertime Amino Acid and Carbohydrate Patterns in Particulate and Dissolved Organic Carbon Across Fram Strait, Front. Mar. Sci., 8, https://doi.org/10.3389/fmars.2021.684675, 2021.

Huang, J., Cai, M., Han, M., Fang, B., Dong, L., Zhang, G., Han, J., Li, S., Rustamova, N., Liu, Y., Li, W., Jiang, H., Huang, J., Cai, M., Han, M., Fang, B., Dong, L., Zhang, G., Han, J., Li, S., Rustamova, N., Liu, Y., Li, W., and Jiang, H.: and functional specialization in extremely arid

ecosystems, 92, 2026.

Jagtap, A., Singh, A., jain, . anand ., Tiwari, M., & Raj, N.: Particulate Organic Matter composition in and around macroalgal beds in Kongsfjorden, Arctic, Zenodo, https://doi.org/https://doi.org/10.5281/zenodo.18457176, 2026.

Jain, A., Krishnan, K. P., Singh, A., Thomas, F. A., Begum, N., Tiwari, M., Bhaskar, V. P., and Gopinath, A.: Biochemical composition of particles shape particle-attached bacterial community structure in a high Arctic fjord, Ecol. Indic., 102, 581–592, https://doi.org/10.1016/j.ecolind.2019.03.015, 2019.

Jiang, H., Lv, Q., Yang, J., Wang, B., Dong, H., Gonsior, M., and Schmitt-kopplin, P.: Organic Geochemistry Molecular composition of dissolved organic matter in saline lakes of the Qing-Tibetan Plateau, Org. Geochem., 167, 104400, https://doi.org/10.1016/j.orggeochem.2022.104400, 2022.

Jo, N., La, H. S., Kim, J. H., Kim, K., Kim, B. K., Kim, M. J., Son, W., and Lee, S. H.: Different Biochemical Compositions of Particulate Organic Matter Driven by Major Phytoplankton Communities in the Northwestern Ross Sea, Front. Microbiol., 12, https://doi.org/10.3389/fmicb.2021.623600, 2021.

Jo, N., Youn, S. H., Joo, H. T., Jang, H. K., Kim, Y., Park, S., Kim, J., Kim, K., Kang, J. J., and Lee, S. H.: Seasonal variations in biochemical (biomolecular and amino acid) compositions and protein quality of particulate organic matter in the Southwestern East/Japan Sea, Front. Mar. Sci., 9, https://doi.org/10.3389/fmars.2022.979137, 2022.

Karl Attard; Rakesh Kumar Singh, J.-P., Gattusof, Karen Filbee-Dexter, Dorte Krause-Jensen, M. K., and Mikael K. Sejr, Philippe Archambault, Marcel Babin, Simon Bélanger, Peter Berg, Ronnie N. Glud, Kasper Hancke, Stefan Jänicke, Jing Qin, Søren Rysgaard, Esben B. Sørensen,

Foucaut Tachon, Frank Wenzhöfer, and M. A.: Seafloor primary production in a changing Arctic Ocean, PNAS, 121, e2303366121, 2024.

Kennedy, J. R. and Blain, C. O.: A systematic review of marine macroalgal degradation: Toward a better understanding of macroalgal carbon sequestration potential, J. Phycol., 61, 399–432, https://doi.org/10.1111/jpy.70031, 2025.

Kim, J., Jo, N., Park, J., Kim, K., Park, S., Kim, Y., Kim, J., Kim, B. K., Lee, B., and Lee, S. H.: Different amino acid compositions and food quality of particulate organic matter driven by two major phytoplankton groups in the Ross Sea, J. Sea Res., 201, 102524, https://doi.org/10.1016/j.seares.2024.102524, 2024.

Krause-Jensen, D. and Duarte, C. M.: Substantial role of macroalgae in marine carbon sequestration, Nat. Geosci., 9, 737–742, https://doi.org/10.1038/ngeo2790, 2016.

Krause-Jensen, D., Archambault, P., Assis, J., Bartsch, I., Bischof, K., Filbee-Dexter, K., Dunton, K. H., Maximova, O., Ragnarsdóttir, S. B., Sejr, M. K., Simakova, U., Spiridonov, V., Wegeberg, S., Winding, M. H. S., and Duarte, C. M.: Imprint of Climate Change on Pan-Arctic Marine Vegetation, Front. Mar. Sci., 7, 1–28, https://doi.org/10.3389/fmars.2020.617324, 2020.

Kuliński et al.: POM sinks and sources in High Arctic Fjords.pdf, 2014.

Kumar, V., Tiwari, M., Nagoji, S., and Tripathi, S.: Evidence of Anomalously Low δ13C of Marine Organic Matter in an Arctic Fjord, Sci. Rep., 6, 1–9, https://doi.org/10.1038/srep36192, 2016.

Kuzyk, Z. Z. A., Macdonald, R. W., Tremblay, J. É., and Stern, G. A.: Elemental and stable isotopic constraints on river influence and patterns of nitrogen cycling and biological productivity in Hudson Bay, Cont. Shelf Res., 30, 163–176, https://doi.org/10.1016/j.csr.2009.10.014, 2010.

Li, H., Zhang, Z., Chen, J., Nair, S., Xiong, T., Zhao, H., He, D., Lee, K., Jiao, N., and Zhang, Y.: Fate and carbon sequestration potential of sunken macroalgae in coastal oceans from long-term microbial degradation perspective, Natl. Sci. Rev., 12, https://doi.org/10.1093/nsr/nwaf273, 2025.

Lobbes, J. M., Fitznar, H. P., and Kattner, G.: Biogeochemical characteristics of dissolved and particulate organic matter, Geochim. Cosmochim. Acta, 64, 2973–2983, 2000.

Machado, M., Machado, S., Pimentel, F. B., Freitas, V., Alves, R. C., and Oliveira, M. B. P. P.: Amino acid profile and protein quality assessment of macroalgae produced in an integrated multi-trophic aquaculture system, Foods, 9, https://doi.org/10.3390/foods9101382, 2020.

Mathew, S., Hong, J. K., Kim, J. H., Chen, M., and Hur, J.: Terrestrial inputs of nutrients and dissolved organic carbon to the Arctic Ocean and their influence on primary production, Mar. Environ. Res., 209, 107182, https://doi.org/10.1016/j.marenvres.2025.107182, 2025.

McGovern, M., Pavlov, A. K., Deininger, A., Granskog, M. A., Leu, E., Søreide, J. E., and Poste, A. E.: Terrestrial Inputs Drive Seasonality in Organic Matter and Nutrient Biogeochemistry in a High Arctic Fjord System (Isfjorden, Svalbard), Front. Mar. Sci., 7, 1–15, https://doi.org/10.3389/fmars.2020.542563, 2020.

van der Mheen, M., Wernberg, T., Pattiaratchi, C., Pessarrodona, A., Janekovic, I., Simpkins, T., Hovey, R., and Filbee-Dexter, K.: Substantial kelp detritus exported beyond the continental shelf by dense shelf water transport, Sci. Rep., 14, 1–12, https://doi.org/10.1038/s41598-023-51003-5, 2024.

Niedzwiedz, S., Voigt, C., Andersen, S., Diehl, N., Descôteaux, R., Damsgård, B., and Bischof, K.: Biochemistry of Arctic kelp specimens is conditioned by the local environment, Mar. Environ. Res., 212, https://doi.org/10.1016/j.marenvres.2025.107604, 2025.

Norkko, A., Thrush, S. F., Cummings, V. J., Gibbs, M. M., Andrew, N. L., Norkko, J., and Schwarz, A. M.: Trophic structure of coastal Antarctic food webs associated with changes in sea ice and food supply, Ecology, 88, 2810–2820, https://doi.org/10.1890/06-1396.1, 2007.

Ørberg, S. B., Duarte, C. M., Geraldi, N. R., Sejr, M. K., Wegeberg, S., Hansen, J. L. S., and Krause-Jensen, D.: Prevalent fingerprint of marine macroalgae in arctic surface sediments, Sci. Total Environ., 898, https://doi.org/10.1016/j.scitotenv.2023.165507, 2023.

Ortega, A., Geraldi, N. R., Alam, I., Kamau, A. A., Acinas, S. G., Logares, R., Gasol, J. M., Massana, R., Krause-Jensen, D., and Duarte, C. M.: Important contribution of macroalgae to oceanic carbon sequestration, Nat. Geosci., 12, 748–754, https://doi.org/10.1038/s41561-019-0421-8, 2019.

Pedersen, M. F., Filbee-Dexter, K., Frisk, N. L., Sárossy, Z., and Wernberg, T.: Carbon sequestration potential increased by incomplete anaerobic decomposition of kelp detritus, Mar. Ecol. Prog. Ser., 660, 53–67, https://doi.org/10.3354/meps13613, 2021.

Pessarrodona, A., Assis, J., Filbee-Dexter, K., Burrows, M. T., Gattuso, J. P., Duarte, C. M., Krause-Jensen, D., Moore, P. J., Smale, D. A., and Wernberg, T.: Global seaweed productivity, Sci. Adv., 8, https://doi.org/10.1126/sciadv.abn2465, 2022.

Pineault, S., Tremblay, J. É., Gosselin, M., Thomas, H., and Shadwick, E.: The isotopic signature of particulate organic C and N in bottom ice: Key influencing factors and applications for tracing the fate of ice-algae in the Arctic Ocean, J. Geophys. Res. Ocean., 118, 287–300, https://doi.org/10.1029/2012JC008331, 2013.

Rantanen, M., Karpechko, A. Y., Lipponen, A., Nordling, K., Hyvärinen, O., Ruosteenoja, K., Vihma, T., and Laaksonen, A.: The Arctic has warmed nearly four times faster than the globe since 1979, Commun. Earth Environ., 3, 1–10, https://doi.org/10.1038/s43247-022-00498-3,

2022.

Renaud, P. E., Løkken, T. S., Jørgensen, L. L., Berge, J., and Johnson, B. J.: Macroalgal detritus and food-web subsidies along an Arctic fjord depth-gradient, Front. Mar. Sci., 2, 1–15, https://doi.org/10.3389/fmars.2015.00031, 2015.

Roy, B.: Tracing Macroalgal-Induced Changes in Carbon Dynamics of High-Arctic Fjords Using Biomarker Fingerprinting, https://doi.org/10.1029/2024JC021900, 2025.

Schimani, K., Zacher, K., Jerosch, K., Pehlke, H., Wiencke, C., and Bartsch, I.: Video survey of deep benthic macroalgae and macroalgal detritus along a glacial Arctic fjord: Kongsfjorden (Spitsbergen), Polar Biol., 45, 1291–1305, https://doi.org/10.1007/s00300-022-03072-x, 2022.

Schimani Katherina: Macroalgal communities in Kongsfjorden, Spitsbergen, 2019.

Singh, A., Pal, B., and Singh, K. S.: Carbohydrate and pigment composition of macroalgae in a kelp-dominated Arctic fjord, Reg. Stud. Mar. Sci., 77, 103644, https://doi.org/10.1016/j.rsma.2024.103644, 2024a.

Singh, A., Jain, A., Singh, R., Singh, K. S., Roy, B., Tiwari, M., David T., D., and Jagtap, A.: Tracing marine and terrestrial biochemical signatures of particulate organic matter in an Arctic fjord (Kongsfjorden), Mar. Chem., 267, 104468, https://doi.org/10.1016/j.marchem.2024.104468, 2024b.

Smale, D. A., Pessarrodona, A., King, N., and Moore, P. J.: Examining the production, export, and immediate fate of kelp detritus on open-coast subtidal reefs in the Northeast Atlantic, Limnol. Oceanogr., 67, S36–S49, https://doi.org/10.1002/lno.11970, 2022.

Stanca, E. and Parsons, M. L.: Examining the dynamic nature of epiphytic microalgae in the Florida Keys: What factors influence community composition?, J. Exp. Mar. Bio. Ecol., 538, https://doi.org/10.1016/j.jembe.2021.151538, 2021.

Taylor Simpkins, Mirjam Van Der Mheen, Morten F. Pedersen, A. P. and Chari Pattiaratchi, Thomas Wernberg, K. F.-D.: Macroalgae detritus decomposition and cross-shelf carbon export from shallow and deep reefs, https://doi.org/10.1002/lno.70006, 2025.

Tselepides, A., Polychronaki, T., Marrale, D., Akoumianaki, I., Dell'Anno, A., Pusceddu, A., and Danovaro, R.: Organic matter composition of the continental shelf and bathyal sediments of the Cretan Sea (NE Mediterranean), Prog. Oceanogr., 46, 311–344, https://doi.org/10.1016/S0079-6611(00)00024-0, 2000.

Upreti, G. C., Ratcliff, R. A., and Riches, P. C.: Protein Estimation in Tissues Containing High Levels of Lipid : Modifications to Lowry ' s Method of Protein Determination Effect of Detergents upon NADPH- Generating Enzymes Protein Estimation by the BCA Method, 427, 421–427, 1988.

Velázquez-Ochoa, R., Ochoa-Izaguirre, M. J., and Soto-Jiménez, M. F.: An analysis of the variability in δ13C in macroalgae from the Gulf of California: Indicative of carbon concentration mechanisms and isotope discrimination during carbon assimilation, Biogeosciences, 19, 1–27, https://doi.org/10.5194/bg-19-1-2022, 2022.

Vidal: Lateral Transport of N-Rich Dissolved Organic Matter Strengthens Phosphorus Deficiency in Western Subtropical North Atlantic, 2018.

Watanabe, K., Yoshida, G., Hori, M., Umezawa, Y., Moki, H., and Kuwae, T.: Macroalgal metabolism and lateral carbon flows create extended atmospheric CO_2 sinks, Biogeosciences Discuss., 1–25, 2019.

Williams: Biological soil crusts of Arctic Svalbard and of Livingston Island, Antarctica, 2017.

Wilson: The contribution of macroalgae-associated fishes to small-scale tropical reef.pdf, 2022.

Woelfel, J., Eggert, A., and Karsten, U.: Marginal impacts of rising temperature on Arctic

benthic microalgae production based on in situ measurements and modelled estimates, Mar. Ecol. Prog. Ser., 501, 25–40, https://doi.org/10.3354/meps10688, 2014.

Yang, J., Jiang, H., Liu, W., Huang, L., Huang, J., and Wang, B.: Potential utilization of terrestrially derived dissolved organic matter by aquatic microbial communities in saline lakes, ISME J., 2313–2324, https://doi.org/10.1038/s41396-020-0689-0, 2020.

Yao, X., Fan, T., Gao, G., Liu, L., Chao, J., and Liu, H.: Spatiotemporal pattern and biodegradation process of amino acids in the large shallow eutrophic lake Taihu, China, Environ. Sci. Pollut. Res., 30, 12584–12595, https://doi.org/10.1007/s11356-022-23014-8, 2023.

Zhu, Z. Y., Wu, Y., Liu, S. M., Wenger, F., Hu, J., Zhang, J., and Zhang, R. F.: Organic carbon flux and particulate organic matter composition in Arctic valley glaciers: Examples from the Bayelva River and adjacent Kongsfjorden, Biogeosciences, 13, 975–987, https://doi.org/10.5194/bg-13-975-2016, 2016.